Resolving the Redundancy of a Seven DOF Wearable Robotic System Based on Kinematic and Dynamic Constraint

Hyunchul Kim, Zhi Li, Dejan Milutinović and Jacob Rosen

Abstract— **According to the seven degrees of freedom (DOFs) human arm model composed of the shoulder, elbow, and wrist joints, positioning of the wrist in space and orientating the palm is a task requiring only six DOFs. Due to this redundancy, a given task can be completed by multiple arm configurations, and there is no unique mathematical solution to the inverse kinematics. The redundancy of a wearable robotic system (exoskeleton) that interacts with the human is expected to be resolved in the same way as that of the human arm. A unique solution to the system's redundancy was introduced by combining both kinematic and dynamic criteria. The redundancy of the arm is expressed mathematically by defining the swivel angle: the rotation angle of the plane including the upper and lower arm around a virtual axis connecting the shoulder and wrist joints which are fixed in space. Two different swivel angles were generated based on kinematic and dynamic constraints. The kinematic criterion is to maximize the projection of the longest principle axis of the manipulability ellipsoid for the human arm on the vector connecting the wrist and the virtual target on the head region. The dynamic criterion is to minimize the mechanical work done in the joint space for each two consecutive points along the task space trajectory. These two criteria were then combined linearly with different weight factors for estimating the swivel angle. Post processing of experimental data collected with a motion capturing system indicated that by using the proposed synthesis of redundancy resolution criteria, the error between the predicted swivel angle and the actual swivel angle adopted by the motor control system was less then five degrees. This result outperformed the prediction based on a single criteria.**

I. INTRODUCTION

The ability to combine human capabilities with robotic-machines has many important applications. Recent improvements in assistive robotic systems [1][2] help people who suffer from a variety of neuromuscular diseases [3]. Unlike the robots designed for tasks that require large forces or moments, assistive robots such as the wearable exoskeleton robot [1] directly interact with humans to enhance or support natural body movement. In order to provide synchronized movement with human users, the control mechanism of assistive robots must incorporate knowledge of natural human movement, which possesses a large degree of flexibility that allows for performing a particular motor task in various postures. The flexibility in the human motion, which results from the neuromuscular and skeletal systems, enable complicated motor skills such as the reaching and grasping motion of the human arm, as well as collision avoidance in object manipulation. In spite of the kinematic redundancy in human arm, healthy humans tend to follow a common pattern when naturally performing the same motor task [4][5]. This research intends to resolve the redundancy in a wearable robotic system (exoskeleton) such that it will be able to render motions as natural as that of the human arm, for the same motor task [6][7].

Previous research has been done on a number of redundancy resolutions. One line of these researches suggested the posture-based motion control strategies [8][9] based on Donders' law, which was originally proposed for eye movements. Most of the related work resolved the redundancy at the kinematic level and focused on the desired hand posture given the kinematic constraint of a target location. Another line of research resolved the redundancy of the human arm based on dynamic constraints, such as the amount of work and energy consumption [10][11]. In this context, the minimum-torque-change model is presented in [12][13]. More recently in [11], it is shown that arm posture based on a particular target is affected by both the kinematics and dynamics, and their relative contribution might be variable depending on the task complexity. Kang et al. [10] presented an inverse kinematic solution which defines the elbow rotation axis for natural arm movement by minimizing the total work done by joint torques for each time step. All criteria discovered thus far are important from an engineering point of view; and they partially explain the human arm inverse kinematic mechanism. However, due to the fundamental differences between robots and humans, it is difficult to fully model human arm movement using these criteria. In [11] it is pointed out that a single criterion cannot explain the human kinematic mechanism. It is recommended that both kinematic and dynamic constraints be constructively unified for a complete description of arm movement.

In this paper, the redundancy of the human arm represented as swivel angle is resolved for the seamless integration between a human and a wearable robot, based on a new kinematic constraint combined with well known dynamic constraint [10]. The proposed algorithm focuses on the functional difference between robot and human manipulators by closely observing human behavior and linearly combines the kinematic and dynamic aspect of the human arm movement to improve the estimation result. In practice, the estimation result can be fed into the wearable robotic system to create the synchronous movement with the human arm for the given end effector position.

II. SYSTEM MODEL AND METHOD

The synchronous movement between the exoskeleton robot and human arm can be guaranteed only when there exists a proper interface between the two. In the following sections, the robotic system supporting natural human arm movements will be briefly described and the redundancy of the human arm for the unconstrained simple reaching task will be analyzed.

A. Exoskeleton Design Supporting Human Arm Model

The kinematics and dynamics of the human arm during activities of daily living (ADL) were previously studied to determine the specifications for the exoskeleton design [Fig.1(a)] [1][14]. Articulation of the exoskeleton is achieved by seven single-axis revolute joints which support 99% of the range of motion required to perform daily activities [1]. Three revolute joints are responsible for shoulder abduction-adduction, flexion-extension and internal-external rotation. A single rotational joint is employed at the elbow, creating elbow flexion-extension. Finally, the lower arm and hand are connected by a three-axis spherical joint resulting in wrist pronation-supination, flexion-extension, and radial-ulnar deviation. As a human-machine interface (HMI), four six-axis force/torque sensors (ATI Industrial Automation, model-Mini40) are attached to the upper arm, the lower arm, the hand and the

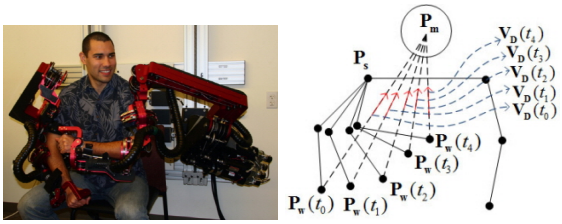

(a) (b)

Fig. 1. a) The seven-DOF exoskeleton supports 99% of the ranges of motion required to preform daily activities. b) Virtual destination for the given wrist position at any time t_i. $V_D(t_i)$ means the virtual destination formed at any time t_i depending on the wrist position $P_W(t_i)$.

tip of the exoskeleton [15]. The force/torque sensor at the tip of the exoskeleton allows measurement of interactions between the exoskeleton and the environment.

B. Human Arm Model: The Extra Degree of Freedom

Since the seven-DOF arm model is redundant, the location and orientation of the hand does not fully specify the configuration of the arm. The configuration becomes fully defined when the elbow position is specified. According to the frame definition in Fig. 2(a), the elbow position introduces three additional variables, but if the wrist position is known, a single variable specifies its position. The arm forms a triangle with a point at the shoulder (P_s) one at that the elbow (P_e) and the last at the wrist (P_w). Both the shoulder and wrist joints are spherical, and allow rotation of point P_e around the vector $(P_w - P_s)$ [Fig. 2(b)]. A local coordinate system at the center of the elbow circle (P_c), gives a reference to measure the swivel angle (ϕ) of the elbow. A normal vector that points in the direction of $(P_w - P_s)$ is defined as:

$$\vec{n} = \frac{P_w - P_s}{||P_w - P_s||} \tag{1}$$

A normalized vector that is projected onto the plane normal to $\vec{n}$ is given by:

$$\vec{u} = \frac{\vec{a} - (\vec{a}\cdot\vec{n})\vec{n}}{||\vec{a} - (\vec{a}\cdot\vec{n})\vec{n}||} \tag{2}$$

where $\vec{a}$ can be selected as any vector. Badler and Torlani [16] suggest $\vec{a}$ to be the $\vec{z}$ vector. This selection has real physical meaning. When ϕ is equal to zero,i.e., the elbow is at its lowest possible point. The last vector of the coordinate system ($\vec{v}$), is found by taking the cross product of $\vec{n}$ and $\vec{u}$. Vectors $\vec{n}$, $\vec{u}$ and $\vec{v}$ form an orthonormal coordinate system. Where $\vec{u}$ and $\vec{v}$ are in the plane of the elbow circle [Fig. 2(c)]. The radius (R) and center (P_c) of the circle are easily found through geometry.

$$R = U\sin(\alpha) \tag{3}$$

$$P_c = P_s + U\cos(\Omega)\cdot\vec{n} \tag{4}$$

$$\cos(\Omega) = \frac{U^2 - L^2 - ||P_w - P_s||^2}{-2L^2||P_w - P_s||} \tag{5}$$

Where U and L are the lengths of the upper and lower arm segments [Fig. 2(b)]. The position of the elbow can now be expresses as a function of ϕ [6].

$$P_e = R[\cos(\phi)\vec{u} + \sin(\phi)\vec{v}] + P_c \tag{6}$$

Then the inverse kinematics for the seven-DOF exoskeleton robot can be solved by the two following equations:

$$T_1T_2T_3T_4T_5T_6T_7g_{st} = g_d \tag{7}$$

$$T_1T_2P_{e_o} = P_e(\phi) \tag{8}$$

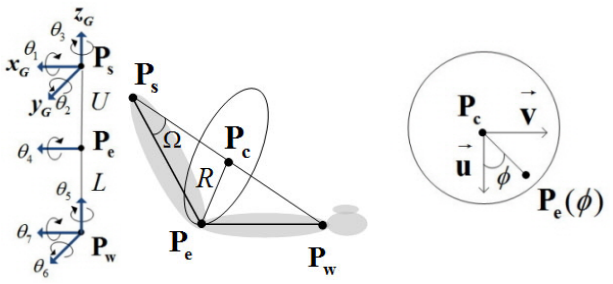

(a) (b) (c)

Fig. 2. a) The global reference frame F_G defined on P_s and joint angles $[\theta_1, \theta_2, \ldots \theta_7]$ for each joint in an initial position of the right arm. b) The extra degree of freedom is defined by a rotation axis that goes from the shoulder to the wrist. c) By creating a coordinate frame at the center of the elbow circle, the swivel angle can be defined allowing the parameterizations of the elbow position by a single variable.

Where T_i is the 4×4 transformation matrix from the link frame $i-1$ to i, g_{st} is the transformation matrix from the seventh link frame to the end effector frame, g_d is the transformation matrix that represents the desired end effector position and orientation, P_{e_o} is the initial position of the elbow, and P_e is from Eq. 6. It is fairly straightforward to solve for the joint angles from this system of equations [17].

III. SWIVEL ANGLE ESTIMATION

In the previous section, we showed that the redundancy of the human arm is defined as the swivel angle. The scope of the research is limited to the swivel angle estimation for the unconstrained and natural reaching/grabbing activity of the human arm. Note that the unconstrained reaching/grabbing task means that there are no obstacles between the human and the target.

The overall estimation mechanism follows the concept of combining two different swivel angles based on the kinematic and dynamic constraints with different weighting coefficients as follows.

$$\phi_{optimal} = K_1\cdot\phi_{kin} + K_2\cdot\phi_{dyn} \tag{9}$$

where ϕ_{kin} and ϕ_{dyn} denote the swivel angles predicted by the kinematic and dynamic constraints respectively. K_1 and K_2 are the weighting coefficients, representing the contribution of each constraint. To estimate K_1 and K_2, we use a motion capture device to collect and record joint angles associated with a given arm movement task. According to the experimental protocol which will be shown in the following section, subjects repeat a given task for five cycles. We will exploit the first cycle of the data to determine the optimum (K_1, K_2) based on the least square solution. Let $\phi_{act}(t) = K_1\cdot\phi_{kin}(t) + K_2\cdot\phi_{dyn}(t) + n(t)$ where $n(t)$ is the measurement error or noise component of the system. Then if we define column vectors X and Y, and a matrix A as:

$$Y = \begin{bmatrix} \phi_{act}(t_0) \\ \phi_{act}(t_1) \\ \vdots \\ \phi_{act}(t_{N-1}) \end{bmatrix}, \quad A = \begin{bmatrix} \phi_{kin}(t_0) & \phi_{dyn}(t_0) \\ \phi_{kin}(t_1) & \phi_{dyn}(t_1) \\ \vdots & \vdots \\ \phi_{kin}(t_{N-1}) & \phi_{dyn}(t_{N-1}) \end{bmatrix}$$

$$X = \begin{bmatrix} K_1 \\ K_2 \end{bmatrix} \tag{10}$$

The least square solution for the weighting coefficient vector based on Eq.10 is given by:

$$X = (A^TA)^{-1}A^TY \tag{11}$$

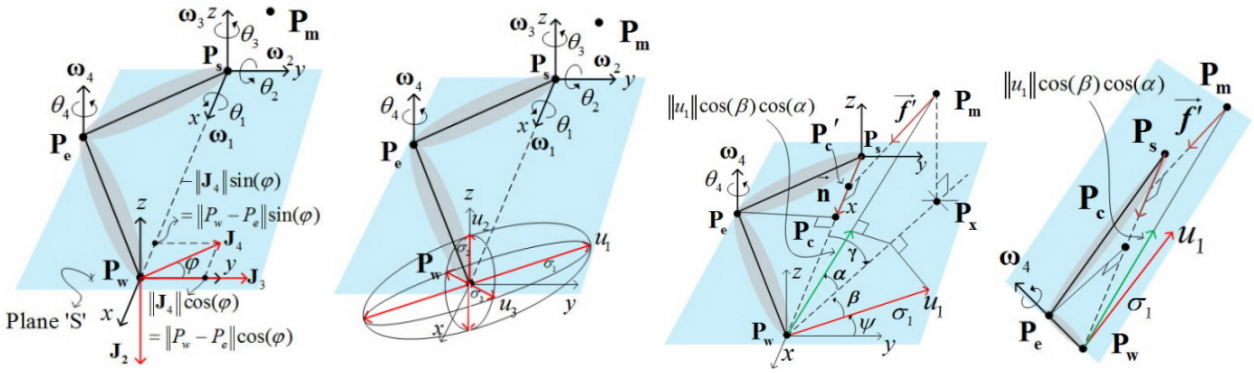

Fig. 3. Body coordinate system composed of P_w, P_e, P_s and P_m. In (c), γ is the angle between $(P_s - P_w)$ and $(P_x - P_w)$ while ψ is the angle between u_1 and y

A. Swivel Angle Based on Kinematic Constraint

Given the role of the head as a cluster of sensing organs and the importance of arm manipulation to deliver food to the mouth, we hypothesize that the swivel angle is selected by the motor control system to efficiently retract the palm to the head region. This hypothesis is supported by the intracortical stimulation experiments to evoke coordinated forelimb movements in the awake primate [18][19]. It has been reported that each stimulation site produced a stereotyped posture in which the arm moved to the same final position regardless of its posture at the initial stimulation. In the most complex example, the monkey formed a frozen pose with the hand in a grasping position in front of the open mouth. This implies that during the arm movement toward an actual target, the virtual target point on the head can be set for the potential retraction of the palm to the virtual target as shown in Fig. 1(b).

1) Manipulability Ellipsoid: According to the above notion of efficient arm movement toward the head, the redundancy of the human arm can be closely associated with manipulability ellipsoid. Let P_m denote the virtual target position at the center of the head in Fig. 3(a). When we consider the combinations of joint velocities satisfying the condition in which $\Sigma_{i=1}^{n} \dot{\theta}_i^{\,2} = 1$, the hand velocity as a function of the joint velocity is described by an ellipsoid that defines the arm's scaled Jacobian. The largest among the major axes of the manipulability ellipsoid defines the direction of the highest sensitivity where the end effector velocity varies in response to the joint space velocity[Fig. 3(b)] [20]. Assuming that virtual hand movement follows the shortest path connecting P_w to P_m, the swivel angle is chosen such that the projection of the major axis of the manipulability ellipsoid onto $(P_m - P_w)$ will be maximized.

Lemma 3.1: Given the inequality $\|P_w - P_s\| > \|P_w - P_e\|$, the longest axis of the manipulability ellipsoid is coplanar with plane S, defined by P_w, P_e and P_s, and its magnitude σ_1 is expressed as

$$\sigma_1 = \sqrt{\lambda_1} = \sqrt{\left(\left(L_{ws}^2 + L_{we}^2\right) + \left(L_{ws}^2 + L_{we}^2\right) c_1\right)/2} \tag{12}$$

$$c_1 = \sqrt{1 - c_2},\ c_2 = 4L_{we}^2 L_{ws}^2 \sin(\varphi)^2 / \left(L_{ws}^2 + L_{we}^2\right)^2$$

Proof: The proof can be found in [21]. ■

2) Optimum Swivel Angle: The optimal swivel angle is defined such that the projection of the longest axis u_1 on the vector $P_m - P_w$ is maximized for the given wrist position. Since we have already shown the detailed description of the optimum swivel angle estimation algorithm in [21], here we only explain the basic idea and the result. Then the optimum swivel angle is :

$$\phi = \underset{\alpha,\beta \in [0\ \ \pi/2]}{\arg\max} \left[u_1^T (P_m - P_w)\right] \tag{13}$$

$$= \underset{\alpha,\beta \in [0\ \ \pi/2]}{\arg\max} \left[\|u_1\| \|P_m - P_w\| \cos(\alpha)\cos(\beta)\right] \tag{14}$$

where α and β are the angles between $(P_m - P_w)$ and plane S, and the angle between u_1 and the projection of $(P_m - P_w)$ onto S [Fig.3(c)], respectively. Note that the projected portion of u_1 onto $(P_m - P_w)$ is represented by $\|u_1\|\cos(\alpha)\cos(\beta)$ and marked as a green arrow in Fig. 3(c). Based on the geometry defined in Fig. 3(c), Eq. 14 is maximized when $\alpha = 0$ regardless of the β determined by the given wrist position. In this condition when $\alpha = 0$, plane S is coplanar with the plane composed by P_m, P_s and P_w as shown in Fig. 3(d). Then the swivel angle under this condition is calculated given the known positions P_m, P_w and P_s. In order to do so, a new vector $\vec{f} = P_w - P_m$ is defined. The vector $\vec{f}'$ is the projection of $\vec{f}$ on the direction of $P_w - P_c'$ in Fig. 3(c). Based on the fact that $\vec{f}'$ is parallel to vector $P_e(\phi) - P_c$ when $\alpha = 0$, the swivel angle is estimated by

$$\phi_{kin} = \arctan 2\left(\vec{n} \cdot \left(\vec{f}' \times \vec{u}\right), \vec{f}' \cdot \vec{u}\right) \tag{15}$$

The estimation algorithm is based on a real time solution of the inverse kinematic. The accuracy of the ϕ_{est} estimation was assessed based on experimental results described in the following section.

B. Swivel Angle Based on Dynamic Constraint

Although the estimated swivel angle based on the purely kinematic constraint in Section III-A can provide a good estimation, it is clear that the dynamic aspect of the manipulator affects the joint configuration during the movement. Thus merging the dynamic effect of the human arm movement into the swivel angle estimation can provide an improved estimation result and reveal the contribution of dynamic effect to the redundancy of the human arm movement. In this context, the redundancy of the human arm movement can be resolved by optimizing the cost function at the dynamic level. For instance, [22] proposed to solve the 3D inverse kinematics based on minimizing the magnitude of total work done by joint torques for each time step. This dynamic criteria had generated satisfactory prediction of the joint space trajectory for the fundamental motions of the human arm, such as the shoulder adduction/abduction, the shoulder flexion/extension, the shoulder internal/external and the elbow flexion/extension. To close the gap between the measured and kinematically estimated swivel angle,

minimizing the magnitude of total work criteria will be adopted as a dynamic constraint in this paper. However note that other dynamic criteria can also be used to improve the estimation performance in the future.

To analyze the reaching motion at dynamic level, the dynamic model of the right human arm is rendered via the Autolev package [23], which generates the motion equation by Kane's method [24]. This dynamic model processes seven DOFs (three DOFs for the shoulder, three DOFs for the wrist and one DOF for the elbow motion), with the frame setup in accordance with the EXO-UL7. The Denavit-Hartenberg parameters (DH) for the dynamic model (Table I) are derived via the modified method [25]. Since the analysis of reaching motion in free space focuses on the wrist position of the human arm, the orientation of the human hand in the dynamic model is pre-specified by locking the three DOFs at the wrist joint. The dynamic model parameters are experimentally measured from the individual subject; the center of mass and the inertia matrices are calculated from the weight of subjects according to the regression equations in [26].

$i-1$	i	α_i	a_i	d_i	θ_i
0	1	$\pi/2$	0	0	$\theta_1(t)-32.94^\circ$
1	2	$\pi/2$	0	0	$\theta_2(t)-\pi/2-28.54^\circ$
2	3	$-\pi/2$	0	0	$\theta_3(t)-\pi-53.6^\circ$
3	4	$-\pi/2$	0	$-UL$	θ_4
4	5	$\pi/2$	0	0	$\theta_5+\pi/2$
5	6	$-\pi/2$	0	$-LL$	$\theta_6+\pi/2$
6	7	$\pi/2$	0	0	$\theta_7+\pi$

TABLE I

DENAVIT-HARTENBERG (DH) PARAMETERS FOR THE DYNAMIC MODEL FOR THE RIGHT HUMAN ARM (MODIFIED METHOD).

For a reaching motion in 3D space, the wrist position of a human arm can be uniquely defined by three variables in the task space, while in the joint space there are four joint angles (three for the shoulder motion and one for the elbow motion) available for configuration. Accordingly, the relationship between movement and muscle forces in a musculoskeletal model is based on the four dynamic equations [22] as:

$$T = M\ddot{Q} + C\left(Q,\dot{Q}\right) + G(Q) \tag{16}$$

In Eq. 16, $\ddot{Q} = [\ddot{q_1},\ddot{q_2},\ddot{q_3},\ddot{q_4}]$ and $\dot{Q} = [\dot{q_1},\dot{q_2},\dot{q_3},\dot{q_4}]$, where q_i represents the joint angle for the ith DOF. M, $C\left(Q,\dot{Q}\right)$ and $G(Q)$ represents the matrix of moment of inertia, the centrifugal/coriolis forces and the gravity force respectively. The external force is regarded as zero in this paper since the given task does not involve interacting with an external load. The active and passive joint torque rendered by musculotendinous forces are represented by T. The calculation of work in joint space for each time step depends on the joint torque and the difference in joint angles. Therefore, the work in joint space during the movement interval $[t_k, t_{k+1}]$ can be computed for two different conditions. Since the dynamic constraint adopted in this paper is from the original work done by [26], we briefly include the essential part for the integrity of the paper.

if $T_{i,t_k} \cdot T_{i,t_{k+1}} > 0$,

$$W_i = \frac{(T_{i,t_k} + T_{i,t_{k+1}}) \cdot \Delta q_i}{2} \tag{17}$$

where T_{i,t_k} and $T_{i,t_{k+1}}$ are the torque of the i-th joint at the time t_k and t_{k+1}. $\Delta q_i = (q_{i,t_{k+1}} - q_{i,t_k})$. is the difference of the i-th joint angle during the time interval $[t_k, t_{k+1}]$.

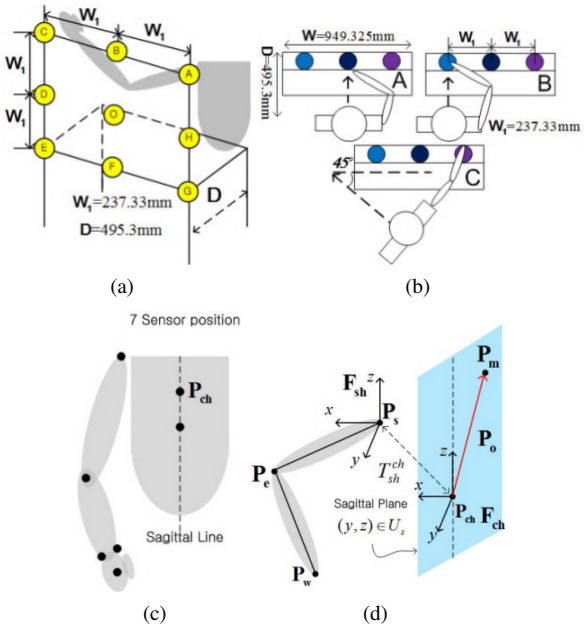

Fig. 4. (a) Hand trajectory for data collection. (b) Top view of three different tasks. Height of table-top to top-of-shelf = 501.65mm, Height of table-top from ground = 736.6mm. (c) Positions of LED markers: Shoulder (Acromioclavicular joint), Elbow (Lateral edge of the Ulna), Wrist (Medial & Lateral edge of the distal end of the radius & ulna), Palm (between 2 & 3 metacarples) and Torso (Upper & lower sternum) d) P_m location with respect to the P_{ch}.

When $T_{i,t_k} \cdot T_{i,t_{k+1}} < 0$,

$$W_i = \frac{(|\Delta q_i| - h_i) \cdot T_{i,t_{k+1}}}{2} - \frac{h_i \cdot T_{i,k}}{2} \tag{18}$$

where $h_i = (|T_{i,t_k}| \cdot |\Delta q_i|)/|T_{i,t_{k+1}} - T_{i,t_k}|$ and has the significance of the difference of the ith joint angle from q_{i,t_k} to the value corresponding to zero crossing of joint torque.

To minimize the work done in joint space for each time step (E.g. $|W|_{t_k,t_{k+1}}$ for the time interval $[t_k, t_{k+1}]$), the swivel angle of the human arm for a specified wrist position trajectory is optimized by the following cost function:

$$C = |W|_{t_k,t_{k+1}} = \sum_{i=1}^{4} |W_i|_{t_k,t_{k+1}} \tag{19}$$

where $|W_i|_{t_k,t_{k+1}}$ denotes the work done by the ith joint.

IV. EXPERIMENTAL PROTOCOL AND RESULTS

In this section, we describe the experimental set up and protocol used to verify the bimodal swivel angle estimation approach introduced in Section III. Using the kinematic data collected from the various reaching tasks, the estimated swivel angle as well as the weighting coefficient will be computed for the data analysis.

A. Experimental Setup and Protocol

The experimental setup is shown in Fig. 4. The kinematic data of the human arm is collected using a motion capture system (Phasespace, Inc.) equipped with eight cameras providing a 240Hz sampling rate and millimeter accuracy at a distance of three meters. To record each joint movement, active LED markers were attached to key anatomical locations: the shoulder, the elbow, the wrist and the chest [Fig. 4(c)].

Five right-handed healthy subjects (three male and two female subjects with an average height of 175 cm and an average age of 29)

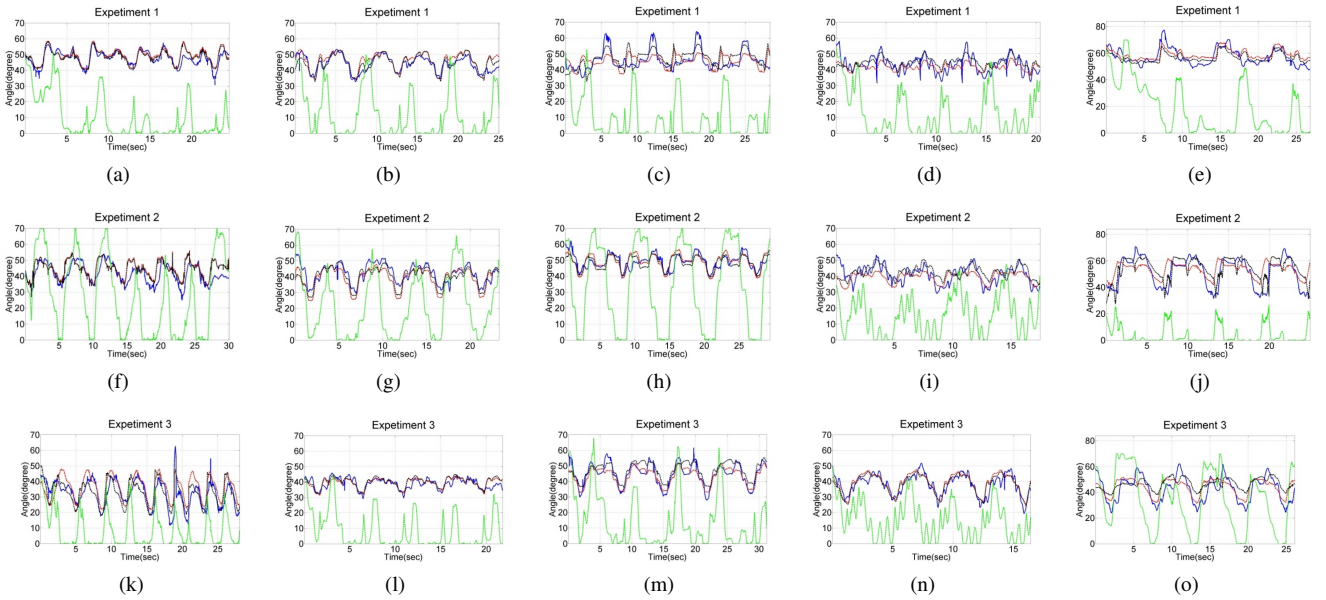

Fig. 5. Comparison between estimated swivel angle(red, green and black line) and measured swivel angle (blue line) for two subjects. Each column corresponds to the result from one of the five subjects. In each row representing one of three different body orientations with respect to targets, there are comparison results for five different subjects. Experiment 1, Experiment 2 and Experiment 3 indicate the estimation results when the center of the chest is aligned with the center of the targets, when the center of the chest is aligned with the leftmost targets and when the center of the chest is rotated by 45 degrees. Blue lines indicate the measured swivel angle. Red, green and black lines indicate the estimated swivel angle based on kinematic constraint, dynamic constraint and combined kinematic and dynamic constraint, respectively.

participated in the experiment. Each subject was asked to reach nine different target locations sequentially and repeatedly (five times) at a self-directed pace as follows [Fig. 4(a)].

$$O \rightarrow A \rightarrow B \rightarrow C \rightarrow D \rightarrow E \rightarrow F \rightarrow G \rightarrow H(5repetitions)$$

The subjects repreated each sequence five times in three different body orientations (A, B, and C, shown in Fig. 4(b)). In orientation A, the center of the subject's chest is aligned with the center of the targets. In orientation B, the center of the subject's chest is aligned with the leftmost targets. And in orientation C, the subject's body is rotated counterclockwise by 45 degrees. The majority of the right arm workspace will be covered in the swivel angle estimation.

B. Optimal Estimation of Target Location (P_m)

Due to anthropometric differences between the subjects, it is desired to locate optimal location of the target (P_m) for each subject. An LED marker located on the chest P_{ch} was used to estimate the target location (P_m). In this experiment the orientation of the torso was restricted, so that the position of P_m as a function of time is represented by

$$P_m(t) = P_{ch}(t) + P_o \tag{20}$$

where P_o is the fixed translation from P_{ch} with respect the global frame as described in Fig. 4(d). The optimal value of P_o is selected such that the difference between $\phi(t)_{est}$ (the estimated swivel angle based on Eq. 15) and $\phi(t)_{act}$ (the calculated swivel angle based on the measured joint positions) is

$$\underset{y,z\in U_s}{\arg\min} \int_y \int_z \left(\int_{t_x}^{t_x+T} |\phi(t)_{act} - \phi(t, P_o(y,z))_{kin}| dt \right) dzdy \tag{21}$$

where U_s is the (y,z) coordinate pairs on the Sagittal plane equally dividing the human body in a vertical plane. Since we assumed that P_m is located on the Sagittal plane, x_{opt} is the same as the x coordinate of $P_{ch}(t)$. For each data set only the first repetition was used for fitting P_o. The actual P_o used for subjects are summarized in Table II. It shows that estimated P_m with respect to the chest position is located on the face, as we expected.

C. Optimum Swivel Angle Estimation

Once the optimum P_m is found, ϕ_{kin} can be easily computed based on Eq. 15. Then the weighting coefficients (K_1, K_2) for both kinematic and dynamic swivel angles were estimated using the one-fifth of the entire experimental data recorded from motion capture system based on Eq. 10. These K_1 and K_2 are applied to the remaining data. The estimated weighting coefficients for each subject are summarized in the third column of Table II. The final form of swivel angle was estimated for the given wrist position data recorded during the experiment and the proposed redundancy resolution criteria. Fig. 5 shows the direct comparison result between the estimated swivel angle and the measured swivel angle indicated by the motor control system of all subjects. The blue, red, green and black lines in Fig. 5 indicate the measured (actual) swivel angle, swivel angle ϕ_{kin} based on kinematic constraint in Eq. 15, swivel angle ϕ_{dyn} based on dynamic constraint in Eq. 19 and combination of two swivel angles based on Eq. 9. The results shows that the ϕ_{dyn} itself does not provide the good estimation result for the unconstrained human arm reaching movement. However by linearly combining ϕ_{dyn} together with ϕ_{kin}, the estimation result was significantly improved. For a more quantitative evaluation of the estimation algorithm, the mean and standard deviation of the estimation errors are listed along the absolute error mean across all the subjects in Table II. The result also shows that the combining ϕ_{dyn} and ϕ_{kin} improved the estimation performance such that mean error for the entire data sets is less than five degrees in all cases with less than four degrees of standard deviation.

V. Conclusion

The proposed swivel angle estimation algorithm is established by linearly combining two different swivel angles generated by

TABLE II
ESTIMATION ERROR

Subject	$P_o(mm)$	K	Mean and Standard Deviation of Absolute Error									
	(x_{opt}, z_{opt})	$(k1, k2)$	Exp 1			Exp 2			Exp 3			For all data
			dyn	kin	comb	dyn	kin	comb	dyn	kin	comb	comb
1	(-160,280)	(0.98,0.02)	37.4°	1.84°	1.72°	10.9°	3.55°	3.33°	21.7°	4.40°	3.61°	3.38±2.44°
2	(-140,320)	(0.97,0.04)	33.37°	2.20°	1.76°	24.86°	3.89°	3.13°	28.10°	2.60°	2.01°	2.45±1.79°
3	(-70,290)	(0.79,0.21)	42.72°	1.35°	0.40°	34.81°	1.71°	0.51°	32.77°	3.440°	0.88°	0.64±0.44°
4	(-140,330)	(0.83,0.17)	31.65°	3.288°	2.79°	27.18°	3.49°	3.48°	23.56°	2.45°	2.35°	2.74±1.98°
5	(-60,220)	(0.86,0.14)	36.53°	3.50°	3.17°	43.47°	6.12°	4.73°	19.19°	5.03°	3.92°	4.59±3.25°

kinematic and dynamic constraints. The estimation algorithm successfully reproduces the natural human arm movement with less than five degrees of estimation error. The result shows that the weighting coefficient for the kinematic constraint is dominant. It is possible that human arm movement defined in our experimental protocol is slow enough to ignore the dynamic effect of the human arm and there exists a common motor control scheme in human based on the kinematic constraint. Although the majority of the estimation comes from the kinematic constraint, it is shown that the dynamic portion of the swivel angle estimation can significantly improve the estimation result. Since the closed form swivel angle estimation based on the kinematic constraint itself provides precise swivel angle estimation performancere with latively low computational complexity, it can be applied to the realtime exoskeleton robot controller. For instance, the algorithm can be applied to the wearable exoskeleton robot (EXO-UL7) in the form of an admittance controller. In doing so, it is expected to significantly reduce the energy exchange between human and robot. For future work, we will extend our experiment and collect more data including object-oriented tasks. By doing this, we expect to reveal the complete seven-DOF human arm movement mechanism.

REFERENCES

[1] J. C. Perry, J. Rosen, and S. Burns, "Upper-limb powered exoskeleton design," *Mechatronics*, vol. 12, no. 4, pp. 408–417, 2007.

[2] T. Nef, M. Guidali, V. Klamroth-Marganska, and R. Riender, "Armin - exoskeleton robot for stroke rehabilitation," in *World Congress on Medical Physics and Biomedical Engineering IFMBE*, vol. 25/9, Munich, Germany, Sept 2009.

[3] H. I. Krebs, M. Ferraro, S. P. Buerger, M. J. Newbery, A. Makiyama, M. Sandmann, D. Lynch, B. T. Volpe, and N. Hogan, "Rehabilitation robotics: pilot trial of a spatial extension for mit-manus," *Journal of NeuroEngineering and Rehabilitation*, Oct 2004.

[4] F. Lacquaniti and J. F. Soechting, "Coordination of arm and wrist motion during a reaching task," *J Neurosci*, vol. 1, pp. 399–408, 1982.

[5] H. Grea, M. Desmurget, and C. Prablanc, "Postural invariance in three-dimensional reaching and grasping movements," *Exp Brain Res*, vol. 134, pp. 155–162, 2000.

[6] D. Tolani, A. Goswami, and N. I. Badler, "Real-time inverse kinematics techniques for anthropomorphic limbs," *Graphical Models and Image Processing*, vol. 62, no. 5, pp. 353–388, Sept. 2000.

[7] S. R. Buss and J.-S. Kim, "Selectively damped least squares for inverse kinematics," *Graphics, gpu, and game tools*, vol. 10, no. 3, pp. 37–49, 2005.

[8] C. Gielen, E. J. Vrijenhoek, T. Flash, and S. Neggers., "Arm position constraints during pointing and reaching in 3-d space," *Journal of Neurophysiology*, vol. 78(2), pp. 660–673, 1997.

[9] ——, "Review of models for the generation of multi-joint movements in 3-d," *Advances in experimental medicine and biology, Progress in Motor Control*, vol. 629, pp. 523–550, 2009.

[10] T. Kang, J. He, and S. I. H. Tillery, "Determining natural arm configuration along a reaching trajectory," *Exp Brain Res*, vol. 167, no. 3, pp. 352–361, 2005.

[11] M. A.Admiraal, M. J. Kusters, and S. C. Gielen, "Modeling kinematics and dynamics of human arm movements," *Motor Control*, vol. 8, no. 3, pp. 312–338, 2004.

[12] Y. Uno, M. Kawato, and R. Suzuki, "Formation and control of optimal trajectory in human multi joint arm movement," *BIOLOGICAL CYBERNETICS*, vol. 61, no. 2, pp. 89–101, 1989.

[13] P. Lee, S. Wei, J. Zhao, and N. I. Badler, "Strength guided motion," *Computer Graphics*, vol. 24, no. 4, pp. 253–262, 1990.

[14] J. C. Perry and J. Rosen, "Design of a 7 degree-of-freedom upper-limb powered exoskeleton," in *IEEE/RAS-EMBS International Conference on Biomedical Robotics and Biomechatronics*, Pisa, Italy, Feb 2006.

[15] L. M. Miller and J. Rosen, "Comparison of multi-sensor admittance control in joint space and task space for a seven degree of freedom upper limb exoskeleton," in *IEEE/RAS-EMBS International Conference on Biomedical Robotics and Biomechatronics*, Tokyo, Japan, Sept 2010.

[16] N. I. Badler and D. Tolani, "Real-time inverse kinematics of the human arm," *Presence*, vol. 5, no. 4, pp. 393–401, 1996.

[17] ——, "Real-time inverse kinematics of the human arm," *IEEE Trans Syst Man, Cybernetics SMC-13*, vol. 5.

[18] R. Dum and P. Strick, *Motor Areas in the frontal Lobe:The Anatomical Substrate for the Central Control of Movement, In Motor Cortex in Voluntary Movements*. CRC press, 2005.

[19] G. M.S, T. C.S, and M. T, "Complex movements evoked by micro stimulation of precentral cortex," *Neuron*, vol. 30;34(5), pp. 841–851, 2002.

[20] A. A. Maciejewski, "Dealing wit the ill-conditioned equations of motion for articulated figures," *IEEE Computer Graphics and Applications*, pp. 63–71, 1990.

[21] H. Kim, L. Miller, and J. Rosen, "Redundancy resolution of a human arm for controlling a seven dof wearable robotic system," in *IEEE international conference on EMBC*, Boston, USA, August 30 September 3 2011.

[22] T. Kang, J. He, and S. I. H. Tillery, "Determining natural arm configuration along a reaching trajectory," *Exp Brain Res*, vol. 167, pp. 352–361, 2005.

[23] M. Genesis, "Autolev." [Online]. Available: http://www.autolev.com/

[24] T. Kane and D. Levinson, *Dynamics: Theory and Applications*. New York: McGraw-Hill, 1985.

[25] J. Craig, *Introduction to Robotics: Mechanics and Control, 3rd edition*. Prentice Hall, 2003, ch. 1.

[26] A. medical research laboratory, "Investigation of inertial properties of human body," Tech. Rep., Mar 1975.